Energy materials

Nitrogen-doped porous 3D graphene with enhanced supercapacitor properties

Hong-Juan Sun[1],* , Bo Liu[2],*, Tong-Jiang Peng[1], and Xiao-Long Zhao[1]

[1] *Key Laboratory of Ministry of Education for Solid Waste Treatment and Resource Recycle, Southwest University of Science and Technology, Mianyang 621010, Sichuan, People's Republic of China*

[2] *School of National Defense Science and Technology, Southwest University of Science and Technology, Mianyang 621010, Sichuan, People's Republic of China*

ABSTRACT

Nitrogen-doped graphene has attracted increasing attention in recent years. Synthesis of nitrogen-doped 3D graphene with high capacitance and excellent capacitive behavior is highly desirable for high-performance supercapacitor applications. In this study, nitrogen-doped porous 3D graphene was prepared from graphite oxide using the mild one-pot hydrothermal procedure. The p-phenylenediamine and ammonia were selected as the reduction and doping agents, respectively. 3D graphene specimens with various nitrogen doping amounts of 6.52–7.81% were prepared. Scanning electron microscopy, transmission electron microscopy, X-ray photoelectron spectroscopy, X-ray diffraction and supercapacitor performance were used to investigate the morphologies, structures and capacitance behaviors of the prepared 3D graphene composites. The results indicated that the as-prepared specimens contained different doping nitrogen amounts. NGP-10.6 showed well-connected 3D porous microstructure with largest doping nitrogen content. In turn, nature and content of nitrogen doping provided the graphene with excellent capacitive behavior. The specific capacitance of NGP-10.6 reached 788 $F \cdot g^{-1}$ at the current density of 0.5 $A \cdot g^{-1}$ and 296 $F \cdot g^{-1}$ at 10 $A \cdot g^{-1}$. Overall, these findings look promising for future applications as outstanding energy storage materials.

Introduction

Supercapacitors are promising and efficient energy storage devices that continue to attract increasing attention due to their excellent electrochemical characteristics [1, 2]. Supercapacitor devices are mainly composed of working electrode, collector, electrolyte, separator and packing material [3]. The electrode material is the most important component affecting the performance of the supercapacitor. The ideal electrode material for supercapacitors should

Hong-Juan Sun and Bo Liu have contributed equally to this work.

Address correspondence to E-mail: sunhongjuan@swust.edu.cn; liuboswust@126.com

have three characteristics: high specific capacitance for improving energy density, excellent rate performance for sustaining high power output and good reversibility of satisfying charge–discharge cycle life [4]. Graphene showed great potential in electrochemical supercapacitors due to its extraordinarily high thermal and electrical conductivity, superior mechanical strength and large specific surface area [5, 6].

Graphene electrode materials obtained by chemical and thermal reductions often show good capacitor performances. However, the strong π–π interactions form agglomerated graphene sheets. This could not provide adequate channels for conduction of electrolyte ions to the electrode material, resulting in moderate capacitor activity and rate capability. To overcome this problem, various functional modifications were performed on graphene [7]. Among these, the formation of three-dimensional graphene aerogel is an effective method. The porous and interconnected three-dimensional structure possesses large specific surface areas and could promote the rapid diffusion of electrolyte ions [8–10]. Three main methods are currently utilized to prepare three-dimensional graphene: self-assembly, template-assisted and direct deposition [11]. The hydrothermal method is the most used method for self-assembly due to simplicity of the reaction conditions and large amounts of synthesized products [12].

Apart from controlling graphene assembly, the other effective means to functionalize and tune assembled graphene is by regulating carbon–carbon bonds within the planar graphene structures [13]. Graphene doping with substituent heteroatoms could prevent restacking of graphene sheets and enhance the electrochemical performance by faradaic reactions [14, 15]. Doping heteroatoms into the graphitic lattice can change the electronic structure and density of state at the Fermi level, overcoming the quantum capacitance limitations of nanocarbon and eventually increasing net specific capacitance [16, 17]. This would lead to high power and energy density [18]. In view of this, nitrogen-doped (N-doped) graphene attracted increasing attention because nitrogen atom has a comparable size to that of carbon, and contains five valence electrons available for forming strong valence bonds with carbon atoms [19]. Promising results with N-doped graphene have been reported under various chemical conditions using multiple nitrogen sources [9]. For example, Jeong et al. [20]

developed a simple chemical method to prepare wearable N-doped rGO supercapacitor electrode with lower resistivity and high capacitance estimated to fourfolds than that of pristine graphene. Zhao et al. [21] successfully prepared ultralight, nitrogen-doped and three-dimensional graphene framework using graphene oxide and pyrrole. The three-dimensional graphene framework-based supercapacitor generated a specific capacitance of 484 $F \cdot g^{-1}$ at the scan rate of 1 $mV \cdot s^{-1}$, which was far superior to that of typical carbon-based electrodes. This was related to the synergetic function of 3D open-pore structure and N-doping. Yue et al. [22] used hydrothermal ammonia reaction to form nanoporous nitrogen-doped graphene film. The specific capacitance of the nanoporous nitrogen-doped graphene film reached 468 $F \cdot g^{-1}$ at 2 $mV \cdot s^{-1}$. Su et al. [23] synthesized 3D nitrogen-doped graphene aerogel nanomeshes with hierarchical porous structures from graphene oxide and urea using iron nitrate as the etching agent. The specific capacitance of this material reached 345.8 $F \cdot g^{-1}$, and the value remained at about 321.0 $F \cdot g^{-1}$ over 2000 cycles at 1.0 $A \cdot g^{-1}$ in 2.0 M KOH.

In this paper, porous nitrogen-doped 3D graphene was prepared by mild one-pot hydrothermal process. Nitrogen-doped graphene samples were readily synthesized using GO as the precursor and p-phenylenediamine (PPD), ammonia ($NH_3 \cdot H_2O$) and PPD + $NH_3 \cdot H_2O$ as nitrogen sources. Small amounts of $NH_3 \cdot H_2O$ in PPD acted as regulator of pH to modify the inner structure of the 3D graphene, improving performance of the supercapacitors. The PPD and $NH_3 \cdot H_2O$ served as sources of nitrogen for graphene doping to generate different nitrogen types. FTIR, XPS, XRD, SEM, TEM and electrochemical testing were applied to investigate the structures, morphologies and electrochemical performances of the obtained 3D nitrogen-doped graphene materials. The products may have potential applications in high-performance supercapacitor applications.

Experimental

Materials

Graphite powder (200 mesh, purity 95.5%) was purchased from Qingdao Shenshu Graphite Manufacturing Plant (Qingdao, China). Analytical-grade $KMnO_4$, H_2SO_4, KOH, p-phenylenediamine (PPD),

36% HCl and 30% H_2O_2 aqueous solutions were purchased from Chengdu Kelong chemicals. All reagents were used as received without further purification. The water used in the experiments was freshly deionized water prepared in our laboratory.

Preparation of graphite oxide

Graphite oxide (GO) was synthesized from flaky graphite powder using the modified Hummers' method [24]. Graphite powder (1.0 g, − 200 mesh) was mixed with concentrated H_2SO_4 (23 mL, 98%) and vigorously stirred in an ice-water bath. Next, $KMnO_4$ (4 g) was slowly added to the mixture while the temperature was kept below 20 °C for 0.5 h. The solution was then stirred for 2 h at 35 °C, and deionized water (80 mL) was slowly added to the mixture and further stirred for 30 min. Finally, H_2O_2 (5%) was added drop-wise to the reaction solution until the solution color turned to yellow. The obtained bright yellow suspension was washed several times with HCl and water until the pH was 7.

Preparation of N-doped three-dimensional graphene

The graphene oxide suspension (GOS) was prepared by ultrasonic dispersion of GO gel in water (2 mg·mL^{-1}) for 2 h. The samples were synthesized by the hydrothermal method. GOS (2 mg·mL^{-1}, 30 mL) and PPD (0.03 g) were mixed in a beaker ultrasonically stirred for 10 min. After adjusting the pH to 10.4, 10.6 and 10.8 using $NH_3 \cdot H_2O$, the mixtures were sealed in a Teflon-lined stainless-steel autoclave and maintained at 180 °C for 12 h. After completion of the reaction, the autoclave was cooled freely to room temperature. The hydrogel products were dried under vacuum at 60 °C for further characterization. The samples synthesized with GOS and PPD were labeled as NGP-PPD (without $NH_3 \cdot H_2O$) and NGP-X (X = 10.4, 10.6, 10.8). The sample synthesized with GOS using only $NH_3 \cdot H_2O$ to adjust the pH to 10.6 was named NGP-NH_3. The specimen synthesized using only GOS was named reduced graphite oxide (RGO).

Characterization

Scanning electron microscopy (SEM) was performed on a ZEISS Ultra 55 microscope. X-ray diffraction (XRD) patterns were measured on a PANalytical X'Pert PRO multifunctional powder diffractometer. X-ray photoelectron spectra (XPS) were obtained using a Kratos XSAM 800 photoelectron spectrometer. Transmission electron microscopy (TEM, Car Zeiss Libra 200FE) was employed to identify the nanoscaled microstructures of the products.

Electrochemical measurements

The obtained NGP-X was first cut into slices (2 mg, 1×1 cm^2). The working electrodes were prepared by pressing the slices onto nickel foam (1×3 cm^2) under 8 MPa for 30 s. The electrodes were then soaked in electrolyte for 2 h before measurements.

The electrochemical testing of the electrodes was performed in a three-electrode cell, containing platinum foil (1.5×1.5 cm^2) as the counter and saturated HgO as the reference electrode, immersed in 6 mol·L^{-1} KOH aqueous solution as the electrolyte. The cyclic voltammetry (CV), galvanostatic charge/ discharge (GCD) and electrochemical impedance spectroscopy (EIS) tests were carried out on a CHI660E electrochemical workstation at room temperature. For CV measurements of NGP-X electrode, the sweep rate was set to 10 mV·s^{-1} within a potential range of − 1.0 to 0 V. For GCD measurements, the current density ranged from 0.5 to 10.0 A·g^{-1} at the same potential range as CV measurements. EIS was tested at 0.01–100 kHz with an amplitude of 5 mV.

Results and discussion

Morphology and microstructure

GO sheets containing hydrophilic edges and hydrophobic basal planes could self-assemble in aqueous media by hydrogen bonding, π–π interactions, electrostatic interactions and coordination to form three-dimensional networks [25].

Except for NGP-PPD, the RGO and NGP-X (X = NH_3, 10.4, 10.6, 10.8) samples displayed well-defined 3D graphene assemblies with cylindrical morphologies (Fig. 1a–c). Among well-defined 3D
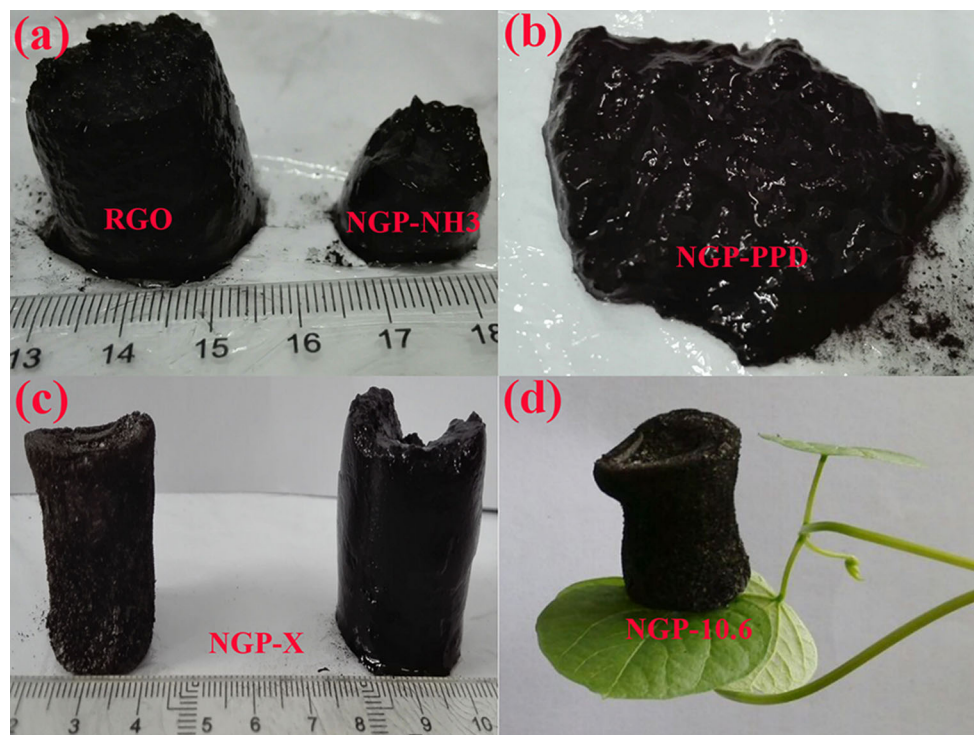
Figure 1 Digital photographs of graphene samples. **a** RGO and NGP-NH$_3$, **b** NGP-PPD, **c** NGP-X ($X = 10.4, 10.6, 10.8$), and **d** NGP-10.6.
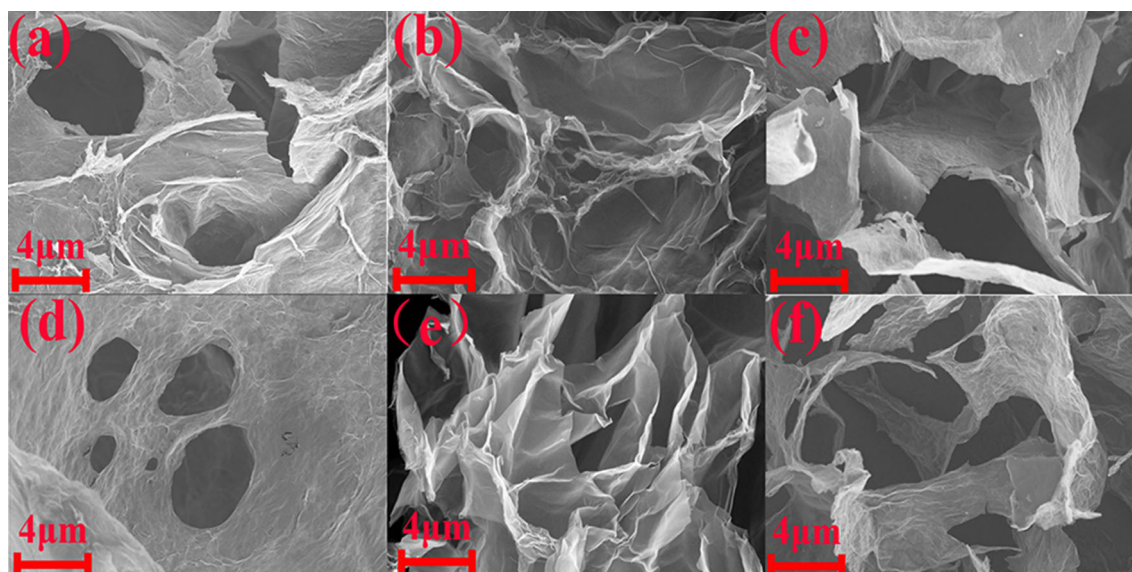

Figure 2 SEM of the prepared graphene samples: **a** RGO, **b** NGP-PPD, **c** NGP-NH$_3$, **d** NGP-10.4, **e** NGP-10.6 and **f** NGP-10.8.

graphene assemblies, NGP-10.6 owned a bulk density of 5.24 cm^3/g and hence could be regarded as ultralight carbon material (Fig. 1d).

The porous microstructures of the as-prepared samples were identified by SEM. As shown in Fig. 2a, RGO was randomly cross-linked with graphene sheets and pores. Also, numerous cracks and broken holes formed in RGO structure. NGP-PPD was stacked with several coiled graphene sheets, gradually evolved into multihole structures (Fig. 2b). After addition of NH$_3$·H$_2$O (Fig. 2c), the aggregation of graphene sheets effectively reduced, producing large

numbers of pores with formed pillared structure thanks to overlapped graphene sheets with each other. Because the ammonia solution replaced some water inside the hydrogel, freezing point of the solution in hydrogel reduced to easily produce more pores during freeze drying. Under the synergistic action of PPD and $NH_3 \cdot H_2O$, C–N covalent bonds between graphene sheets were formed, enhancing the strength of NGP–X (X = 10.4, 10.6, 10.8) samples. In particular, NGP-10.6 showed well-defined and interconnected 3D porous networks with pore sizes ranging from tens to hundreds of nanometers, and pore walls consisting of ultrathin stacked graphene sheets (Fig. 2e). However, at pH around 10.6, the overall compactness was destroyed and the three-dimensional skeleton partly broken, forming numerous broken fragments due to decreased nitrogen contents (Fig. 2f).

Figure 3 illustrates the TEM images of RGO and NGP–X (X = PPD, NH$_3$, 10.4, 10.6, 10.8). All samples appeared highly transparent with gauze-like morphologies. RGO and NGP-PPD samples showed heavy folds and crimped edges due to the weak dispersions and defects present on samples surfaces and edges. After $NH_3 \cdot H_2O$ treatment, the wrinkled degree of graphene surface improved due to the better disperse ability. Notably, NGP-10.6 exhibited better dispersion ability with large ultrathin pore walls, beneficial to electron transport and diffusion of electrolyte ions.
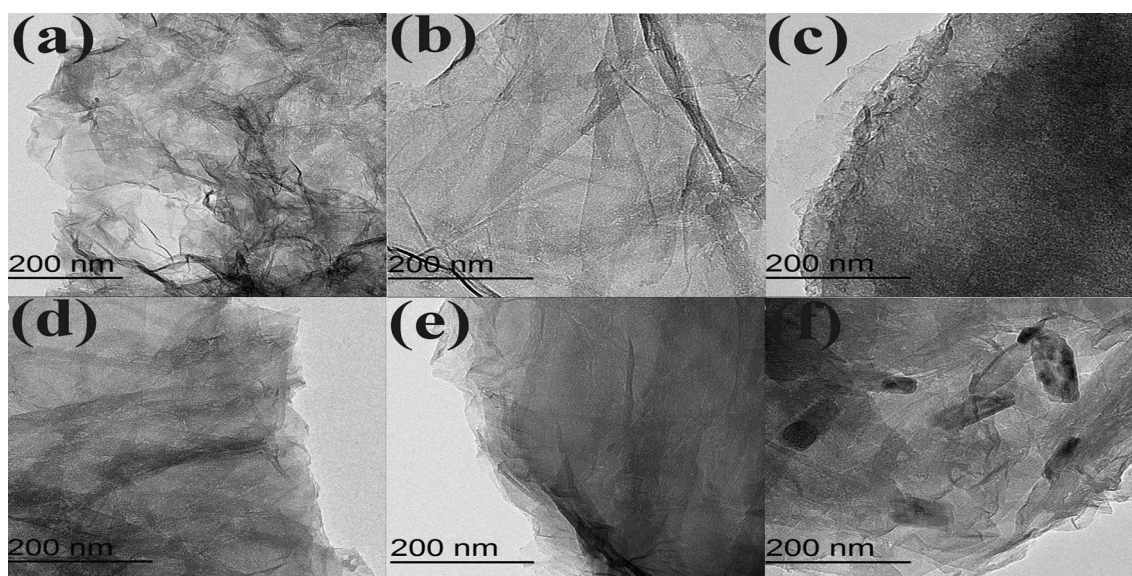
Structural transformation

The diffraction peak at $2\theta = 8.3°$ was attributed to the (001) crystalline plane of GO (Fig. 4), corresponding to an interlayer spacing of approximately 1.06 nm. After the hydrothermal reaction, the diffraction peak vanished due to the removal of oxygen functional groups, suggesting the reduction of GO by hydrothermal reaction. Moreover, a new broad diffraction appeared near 24.8–25.5° with d-space of 0.34–0.37 nm, corresponding to graphite (002) plane. This suggested the recovery of some graphitic crystal structure and π-conjugated system. Addition of single or double N sources in GO declined the d-space
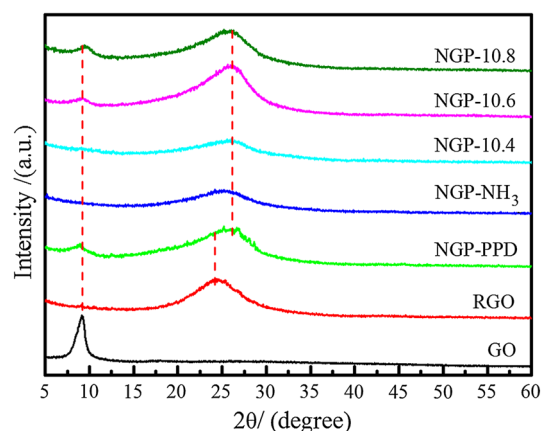

Figure 4 XRD patterns of GO, RGO, and NGP-X (X = PPD, NH$_3$, 10.4, 10.6, 10.8) samples.

Figure 3 TEM of graphene samples: **a** RGO, **b** NGP-PPD, **c** NGP-NH$_3$, **d** NGP-10.4, **e** NGP-10.6 and **f** NGP-10.8.
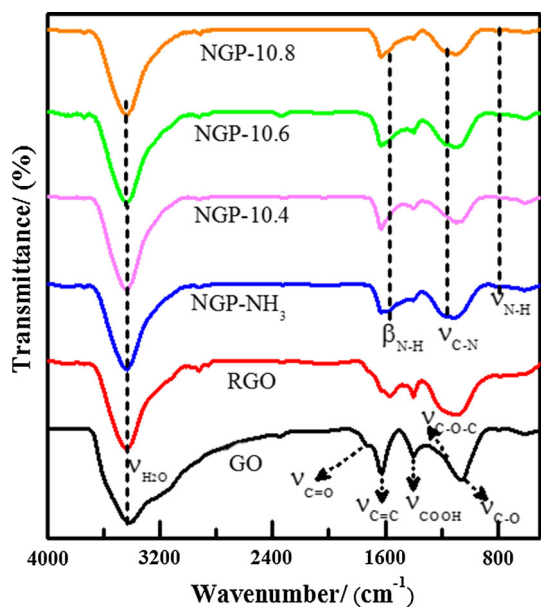
Figure 5 FTIR spectra of GO, RGO, and NGP-X (X = PPD, NH_3, 10.4, 10.6, 10.8) samples.

around 25° when compared to that of RGO, implying that both PPD and $NH_3 \cdot H_2O$ boosted the removal of oxygen functional groups from GO.

Functional properties

As shown in Fig. 5, GO structure contained various oxygen-containing functional groups. The absorption peaks at 3423, 1712, 1630, 1395, 1186 and 1061 cm^{-1} were assigned to the stretching vibrational peaks of H_2O, carboxyl (C=O), aromatic (C=C), carboxylic (COOH), epoxy (C–O–C) and alkoxy (C–O), respectively [26, 27]. Compared to GO, an increase in peak intensities of C=O, C=C, C–O–C, C–O in RGO was observed, indicating that GO was effectively reduced by the hydrothermal process. Compared to RGO, three new absorption peaks appeared at 790, 1163 and 1568 cm^{-1} in NGP-X samples, corresponding to N–H, C–N absorption vibration and N–H bending vibration, respectively. The latter indicated the involvement of PPD molecules during the reaction [28, 29].

Structural bonding mode

To gain a better understanding of the changes in nitrogen contents and existing functional groups, XPS was used to scan the specimens and the results are gathered in Fig. 6. The C1s of GO and RGO showed

no presence of nitrogen (Fig. 6a). GO was mainly composed of epoxy, hydroxyl and carbonyl groups (Fig. 6b). After reduction of GO to RGO, the intensity of the sp^2 C–C peak enhanced (Fig. 6c). This could be attributed to reduction in oxygen-containing groups, favorable for recovery of graphitized C–C bonding. Such transformations were consistent with previous reports [30].

After nitrogen doping, C1s peak of N-doped graphene underwent divisions to form four sub-peaks, belonging to C=C/C–C, C–N, C=O and O–C=O, respectively (Fig. 6d–h). This indicated the formation of covalent bonds between graphene sheets and nitrogen sources (PPD and $NH_3 \cdot H_2O$) [31]. Moreover, the C–N bond appeared as C–O–C/C–O bond vanished, consistent with other studies [32, 33]. The epoxy could react with ammonia, and the addition of PPD or/and $NH_3 \cdot H_2O$ would open the ring of epoxy and then ammonia reacted with C–O to form C–N bonds [34].

The doping nitrogen could be split into numerous peaks with different nitrogen sources (Fig. 7). For NGP-PPD (Fig. 7a), the total nitrogen content was estimated to be 4.89 at.%, and types of doping nitrogen were identified as pyridinic and pyrrolic nitrogens. For NGP-NH_3 (Fig. 7b), the total nitrogen content was recorded as 4.91 at.%, and types of doping nitrogen were based on pyridinic, pyrrolic, graphitic and molecular nitrogens. Among these, molecular nitrogen was formed by insertion of N_2 in graphene sheets during the nitrogen doping reaction. For NGP-X (X = 10.4, 10.6, 10.8), total nitrogen contents were estimated to be 7.65, 7.81 and 6.52 at.%, respectively (Fig. 7c–e). The main nitrogen types were identified as pyridinic, pyrrolic and molecular nitrogens. The addition of $NH_3 \cdot H_2O$ induced molecular nitrogen with significant effects on formation of porous structures.

Supercapacitor performance

The supercapacitor performances of RGO, NGP-PPD, NGP-NH_3 and NGP-X (X = 10.4, 10.6, 10.8) were investigated, and the data are compiled in Fig. 8. The cyclic voltammetry curves performed at 10 mV·s^{-1} showed good rectangle shapes with well-broaden peaks (Fig. 8a), indicating fine electrical double-layer capacitance [35, 36]. NGP-10.6 depicted maximum specific capacitance due to the large area of cyclic voltammetry curve.

Figure 6 C1s spectra of
graphene samples:
a comparison of all spectra,
b GO, **c** RGO, **d** NGP-PPD,
e NGP-NH₃, **f** NGP-10.4,
g NGP-10.6 and **h** NGP-10.8.
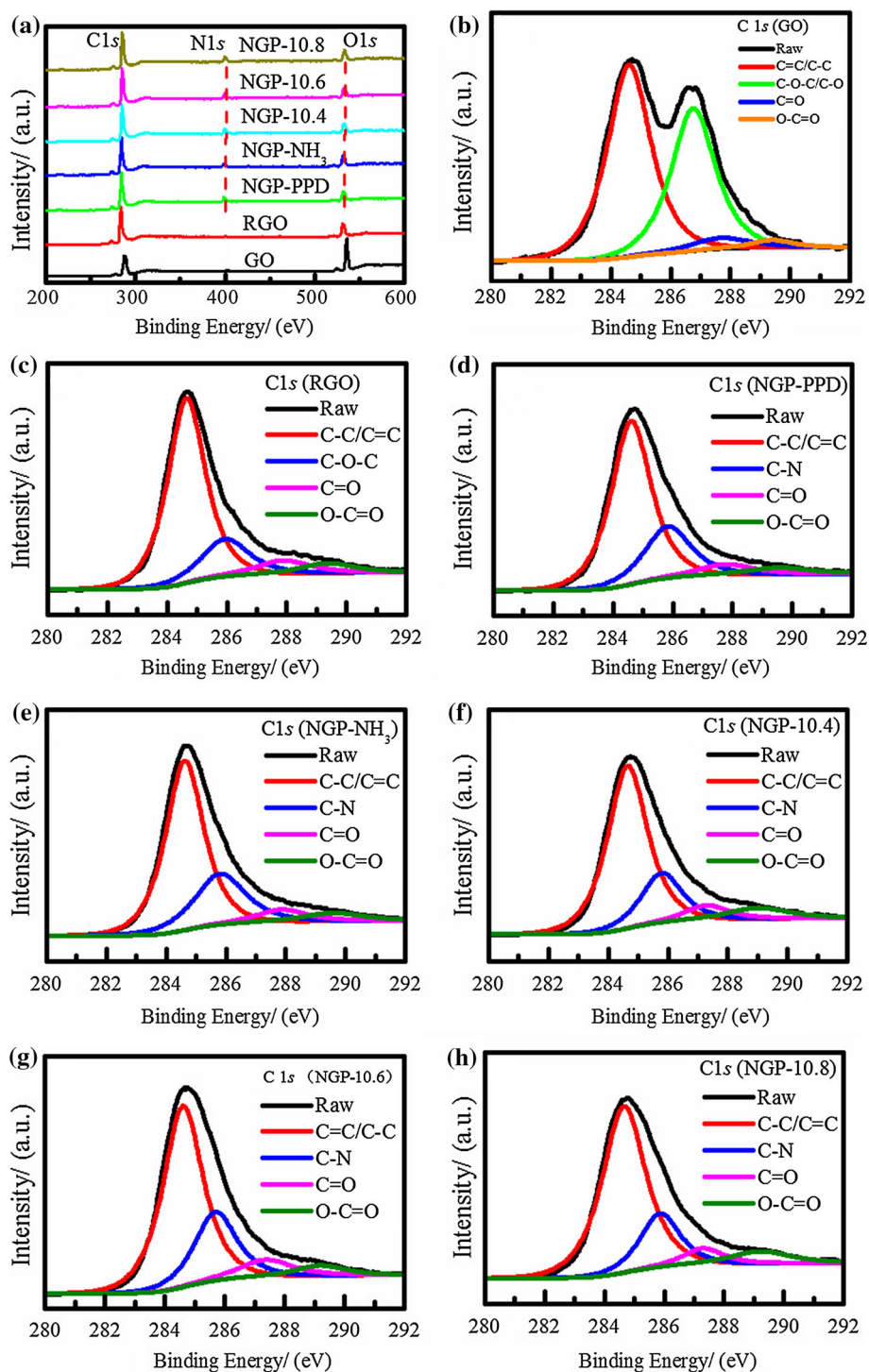
The galvanostatic charge/discharge curves at current density of 1 A·g^{-1} showed good triangle shapes (Fig. 8b), confirming the fine electrical double-layer capacitance. The NGP-10.6-based material showed the best symmetrical isosceles triangle shape with longest charge/discharge time, indicating fast electrochemical reaction and relevant electrochemical reversibility. The specific capacitance value of NGP-10.6 was estimated to be 788 F·g^{-1} at the current density of 0.5 A·g^{-1} (Fig. 8c). The increase in current density to 10 A·g^{-1} reduced the specific capacitance to 296 F·g^{-1}. After 5000 times of charge and discharge

Figure 7 N1 s spectra of graphene samples: **a** NGP-PPD, **b** NGP-NH₃, **c** NGP-10.4, **d** NGP-10.6, **e** and NGP-10.8.
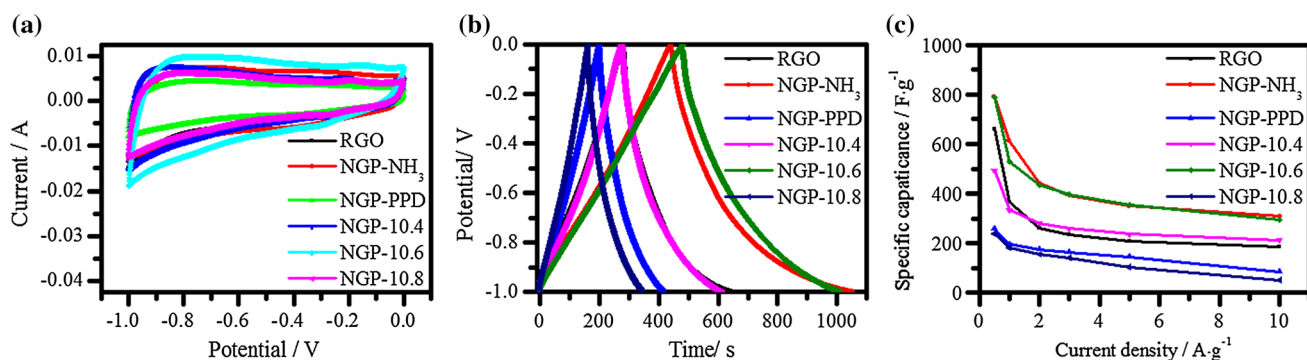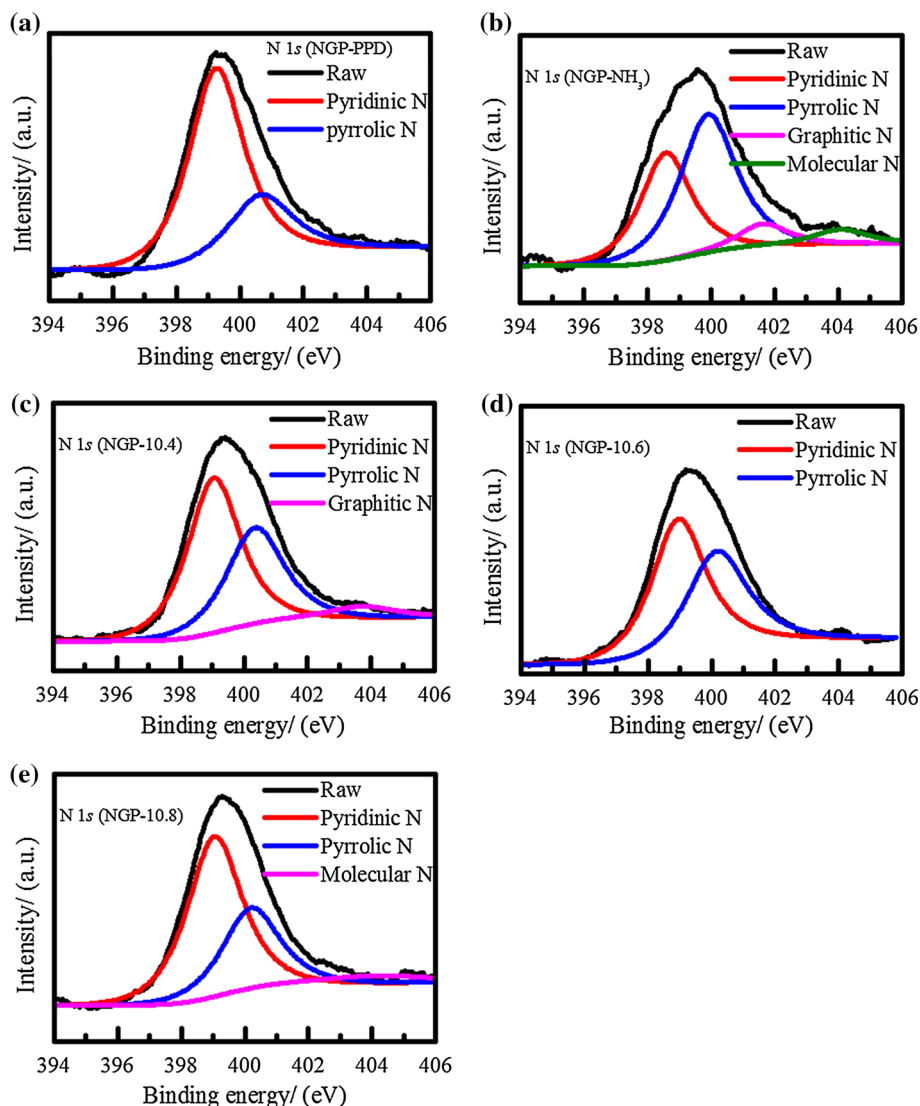

Figure 8 Supercapacitor performances of the as-prepared samples: **a** cyclic voltammetry curves, **b** charge/discharge curves and **c** specific capacitances.

cycles in Fig. 9, the specific capacity retention rate of NGP-10.6 was about 85.4%, showing good electrochemical performance. The specific capacitance of other composites based on 3D graphene and nitrogen-based graphene materials is listed in Table 1. Compared with the specific capacitance reported in

the literature, the result in this study was higher than that of other graphene and conducting polymer-based composites.

The excellent electrochemical performance of NGP-10.6 could be attributed to two factors. From the results of SEM and TEM, the larger fold areas and uniform 3D interconnected porous structure increased the specific surface area of NGP-10.6, benefiting the multidimensional electron transport and accelerating the diffusion of electrolyte ions into the materials. In XPS analysis, with the synergistic effects of PPD and $NH_3 \cdot H_2O$, the NGP-10.6 has the highest content of nitrogen, especially in the pyridinic and pyrrolic nitrogens. The pyridinic nitrogen can

effectively improve the oxidation–reduction reaction. In addition, the pyrrolic nitrogen is a kind of electrochemically active nitrogen. It has electron donor characteristics, which can effectively increase the charge mobility and improve the catalytic activity of carbon in electron transfer reaction. Furthermore, it was reported that the small amount of N-bearing groups of the N-doped graphene could store electronic charges via the redox reactions at the electrode/electrolyte interface, which can in principle enhance the supercapacitor performance. [19].

Conclusions

Nitrogen-doped porous 3D graphene was successfully prepared using the hydrothermal method with PPD and $NH_3 \cdot H_2O$. The morphologies, structures and electrochemical behaviors of the nitrogen-doped porous 3D graphenes were systematically investigated. The nitrogen doping amounts were shown to differ among the prepared samples. NGP-10.6 depicted the largest doping nitrogen content with well-connected 3D porous microstructure. The type and content of doping nitrogen in the material affected the capacitive behavior. Overall, these findings look promising for future development of nitrogen-doped porous 3D graphene materials with large surface areas and uniform porous structures for advanced supercapacitor applications.
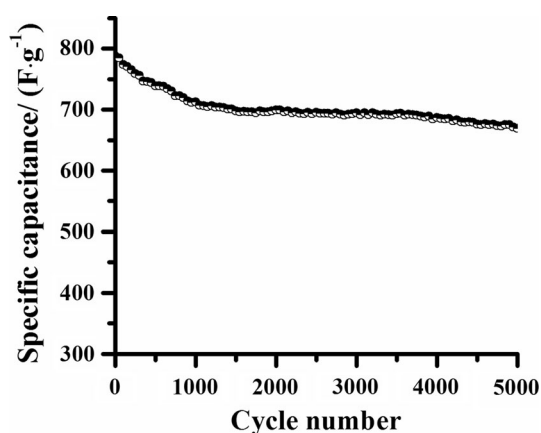

Figure 9 Cycling performance of NGP-10.6 at current density of $0.5 \ A \cdot g^{-1}$.

Table 1 The capacitance of reported 3D graphene and nitrogen-based graphene materials

Sample name	Doping agents	Capacitance	References
Nitrogen-doped graphene nanosheets	Urea	326 $F \cdot g^{-1}$ at a current density of 0.2 $A \cdot g^{-1}$	[37]
Versatile, ultralight, nitrogen-doped graphene framework	Pyrrole	484 $F \cdot g^{-1}$ at a current density of 1 $A \cdot g^{-1}$	[21]
3D nitrogen-doped graphene aerogel	Urea	345.8 $F \cdot g^{-1}$ at a current density of 1 $A \cdot g^{-1}$	[23]
Nitrogen-doped worm-like hierarchical porous carbon	Melamine	178 $F \cdot g^{-1}$ at a current density of 1 $A \cdot g^{-1}$	[38]
Nitrogen-doped graphene aerogel nanomesh	Ammonium hydroxide	290 $F \cdot g^{-1}$ at a current density of 1 $A \cdot g^{-1}$	[39]
Nitrogen-doped porous 3D graphene	p-Phenylenediamine	788 $F \cdot g^{-1}$ at the current density of 0.5 $A \cdot g^{-1}$	This work

Acknowledgements

References

[1] Jiang H, Lee PS, Li C (2012) 3D carbon based nanostructures for advanced supercapacitors. Energy Environ Sci 6:41–53

[2] Iamprasertkun P, Krittayavathananon A, Sawangphruk M (2016) N-doped reduced graphene oxide aerogel coated on carboxyl-modified carbon fiber paper for high-performance ionic-liquid supercapacitors. Carbon 102:455–461

[3] Wang G, Zhang L, Zhang J (2012) A review of electrode materials for electrochemical supercapacitors. Cheminform 41:797

[4] Yu Z, Tetard L, Zhai L, Thomas J (2015) Supercapacitor electrode materials: nanostructures from 0 to 3 dimensions. Energy Environ Sci 8:702–730

[5] Elkady MF, Shao Y, Kaner RB (2016) Graphene for batteries, supercapacitors and beyond. Nature Reviews Materials 1:16033

[6] Ma Z, Tao L, Liu D, Li Z, Zhang Y, Liu Z, Liu H, Chen R, Huo J, Wang S (2017) Ultrafine nano-sulfur particles anchored on in situ exfoliated graphene for lithium-sulfur batteries. J Mater Chem A 5:9412–9417

[7] Yan D, Li Y, Huo J, Chen R, Dai L, Wang S (2017) Defect chemistry of nonprecious-metal electrocatalysts for oxygen reactions. Adv Mater 29:1606459

[8] Gao H, Xiao F, Ching CB, Duan H (2012) High-performance asymmetric supercapacitor based on graphene hydrogel and nanostructured MnO_2. ACS Appl Mater Interfaces 4:2801

[9] Liao Y, Huang Y, Shu D, Zhong Y, Hao J, He C, Zhong J, Song X (2016) Three-dimensional nitrogen-doped graphene hydrogels prepared via hydrothermal synthesis as high-performance supercapacitor materials. Electrochim Acta 194:136–142

[10] Yang Z, Jia L, Yue H, Cheng H, Hu C, Jiang C, Lan J, Cao A, Qu L (2013) Highly compression-tolerant supercapacitor based on polypyrrole-mediated graphene foam electrodes. Adv Mater 25:591

[11] Jiang L, Fan Z (2014) Design of advanced porous graphene materials: from graphene nanomesh to 3D architectures. Nanoscale 6:1922–1945

[12] Qian Y, Ismail IM, Stein A (2014) Ultralight, high-surface-area, multifunctional graphene-based aerogels from self-assembly of graphene oxide and resol. Carbon 68:221–231

[13] Dong X, Hu N, Wei L, Su Y, Wei H, Yao L, Li X, Zhang Y (2016) A new strategy to prepare n-doped holey graphene for high-volumetric supercapacitors. J Mater Chem A 4:9739–9743

[14] Zhang C, Mahmood N, Yin H, Liu F, Hou Y (2013) Synthesis of phosphorus-doped graphene and its multifunctional applications for oxygen reduction reaction and lithium ion batteries. Adv Mater 25:4932–4937

[15] Pettong T, Iamprasertkun P, Krittayavathananon A, Sukha P, Sirisinudomkit P, Seubsai A, Chareonpanich M, Kongkachuichay P, Limtrakul J, Sawangphruk M (2016) High-performance asymmetric supercapacitors of $MnCo_2O_4$ nanofibers and n-doped reduced graphene oxide aerogel. ACS Appl Mater Interfaces 8:34045–34053

[16] Wang Y, Tao L, Xiao Z, Chen R, Jiang Z, Wang S (2018) 3D carbon electrocatalysts in situ constructed by defect-rich nanosheets and polyhedrons from nacl-sealed zeolitic imidazolate frameworks. Adv Func Mater 28:1705356

[17] Guo M, Balamurugan J, Thanh TD, Kim NH, Lee JH (2016) Facile fabrication of Co_2CuS_4 nanoparticle anchored n-doped graphene for high-performance asymmetric supercapacitors. J Mater Chem A 4:17560–17571

[18] Kumar NA, Baek JB (2015) Doped graphene supercapacitors. Nanotechnology 26:492001

[19] Iamprasertkun P, Krittayavathananon A, Seubsai A, Chanlek N, Kidkhunthod P, Sangthong W, Maensiri S, Yimnirun R, Nilmoung S, Pannopard P, Ittisanronnachai S, Kongpatpanich K, Limtrakul J, Sawangphruk M (2016) Charge storage mechanisms of manganese oxide nanosheets and n-doped reduced graphene oxide aerogel for high-performance asymmetric supercapacitors. Sci Rep 6:37560

[20] Jeong HM, Lee JW, Shin WH, Choi YJ, Shin HJ, Kang JK, Choi JW (2011) Nitrogen-doped graphene for high-performance ultracapacitors and the importance of nitrogen-doped sites at basal planes. Nano Lett 11:2472

[21] Zhao Y, Hu C, Hu Y, Cheng H, Shi G, Qu L (2012) A versatile, ultralight, nitrogen-doped graphene framework. Angew Chem 124:11533–11537

[22] Yue S, Tong H, Gao Z, Bai W, Lu L, Wang J, Zhang X (2017) Fabrication of flexible nanoporous nitrogen-doped graphene film for high-performance supercapacitors. J Solid State Electrochem 21:1653–1663

[23] Su XL, Cheng MY, Fu L, Zheng GP, Zheng XC, Yang JH, Guan XX (2017) Facile synthesis of 3D nitrogen-doped graphene aerogel nanomeshes with hierarchical porous structures for applications in high-performance supercapacitors. New J Chem 41:5291–5296

[24] Jr WSH, Offeman RE (1958) Preparation of graphitic oxide. J Am Chem Soc 80:1339

[25] Yoo JJ, Balakrishnan K, Huang J, Meunier V, Sumpter BG, Srivastava A, Conway M, Reddy ALM, Yu J, Vajtai R (2011) Ultrathin planar graphene supercapacitors. Nano Lett 11:1423–1427

[26] Hu C, Yu C, Li M, Wang X, Dong Q, Wang G, Qiu J (2015) Nitrogen-doped carbon dots decorated on graphene: a novel all-carbon hybrid electrocatalyst for enhanced oxygen reduction reaction. Chem Commun 51:3419–3422

[27] Pal K, Panwar V, Bag S, Manuel J, Ahn JH, Kim J (2014) Graphene oxide-polyaniline-polypyrrole nanocomposite for a supercapacitor electrode. RSC Adv 5:3005–3010

[28] Han Z, Tang Z, Li P, Yang G, Zheng Q, Yang J (2013) Ammonia solution strengthened three-dimensional macro-porous graphene aerogel. Nanoscale 5:5462–5467

[29] Wang T, Wang L, Wu D, Xia W, Zhao H, Jia D (2014) Hydrothermal synthesis of nitrogen-doped graphene hydro-gels using amino acids with different acidities as doping agents. J Mater Chem A 2:8352–8361

[30] Yu Y, Zhou M, Shen W, Zhang H, Cao Q, Cui H (2012) Synthesis of electrochemiluminescent graphene oxide functionalized with a ruthenium(II) complex and its use in the detection of tripropylamine. Carbon 50:2539–2545

[31] Kim K, Yang S, Park Y, Lee M, Kim BS, Lee H (2014) Annealing effects after nitrogen ion casting on monolayer and multilayer graphene. J Phys Chem C 117:2129–2134

[32] Wang K, Li L, Zhang T, Liu Z (2014) Nitrogen-doped graphene for supercapacitor with long-term electrochemical stability. Energy 70:612–617

[33] Kumar A, Khandelwal M (2014) Amino acid mediated functionalization and reduction of graphene oxide-synthesis and the formation mechanism of nitrogen-doped graphene. New J Chem 38:491–495

[34] Che J, Shen L, Xiao Y (2010) A new approach to fabricate graphene nanosheets in organic medium: combination of reduction and dispersion. J Mater Chem 20:1722–1727

[35] Chen K, Song S, Liu F, Xue D (2015) Structural design of graphene for use in electrochemical energy storage devices. Chem Soc Rev 44:6230

[36] Xiong G, Meng C, Reifenberger RG, Irazoqui PP, Fisher TS (2014) A review of graphene-based electrochemical micro-supercapacitors. Electroanalysis 26:30–51

[37] Sun L, Wang L, Tian C, Tan T, Xie Y, Shi K, Li M, Fu H (2012) Nitrogen-doped graphene with high nitrogen level via a one-step hydrothermal reaction of graphene oxide with urea for superior capacitive energy storage. RSC Adv 2:4498–4506

[38] Liu Z, Xiao K, Guo H, Ning X, Hu A, Tang Q, Fan B, Zhu Y, Chen X (2017) Nitrogen-doped worm-like graphitized hierarchical porous carbon designed for enhancing area-normalized capacitance of electrical double layer supercapacitors. Carbon 117:163–173

[39] Su XL, Fu L, Cheng MY, Yang JH, Guan XX, Zheng XC (2017) 3D nitrogen-doped graphene aerogel nanomesh: facile synthesis and electrochemical properties as the electrode materials for supercapacitors. Appl Surf Sci 426:924–932